energies

MDPI

Article

Comparison of Cooling Systems in Power Plant Units

Alexander Genbach [1], Hristo Beloev [2] and David Bondartsev [1,*]

[1] Heat & Power Units Department, Almaty University of Power Engineering and Telecommunications, 050013 Almaty, Kazakhstan; a.genbach@aues.kz
[2] Department of Agricultural Machinery, University of Ruse Angel Kanchev, 7017 Ruse, Bulgaria; hbeloev@uni-ruse.bg
* Correspondence: d.bondartsev@aues.kz

Abstract: A new porous system in power plants allowing the management of the crisis of heat exchange at boiling water in porous structures has been investigated. This study refers to the thermal power plants of electrical power stations and devices for cutting natural and artificial mineral media. Combustion chambers and supersonic nozzles were cooled by different porous structures. The optimum cell sizes of the porous structures were determined and data on the heat transfer capacity for the (critical) heat flow were obtained. A thermal device in the form of a rocket-type burner with a detonation jet showed high efficiency for capillary-porous and flow-through cooling systems. The economic effect per burner is not less than 200–300 dollars, and the coolant consumption is reduced by dozens of times, which is environmentally important. A comparative evaluation of the investigated structures and coatings has advantages over other cooling systems. The integration of mesh structures with capillary-porous coatings of natural mineral media produces a synergistic effect of combining them into a technology of their manufacturing, the expansion of critical loads removal and control of the limit state of the coatings.

Keywords: natural materials; capillary-porous coatings and structures; capillary-porous system; combustion chamber; boiling crisis

Citation: Genbach, A.; Beloev, H.; Bondartsev, D. Comparison of Cooling Systems in Power Plant Units. *Energies* **2021**, *14*, 6365. https://doi.org/10.3390/en14196365

Academic Editors: Alessia Arteconi, Magdalena Piasecka, Márta Rencz and Ron Zevenhoven

Received: 31 July 2021
Accepted: 27 September 2021
Published: 5 October 2021

1. Introduction

Cooling systems [1–5] or thermal protection [6] play the most important role in ensuring reliable and highly economical operation of power plants. They cool the hottest and most stressed components and maintain the calculated thermal stress level of the parts. Ultimate turbine inlet temperature, due to excessive wall temperature, is a problem in hypersonic vehicles [1,6]. There is a similar problem in steam turbines at supercritical steam parameters [3]. In [4], seven different cooling schemes for gas turbine blade cooling are analyzed, which are ineffective if the gas temperature rises further.

Research and development work is being actively carried out on cooling systems of the power equipment used in power plants, in order to achieve high overall efficiency [7–15], but the task of further increasing the initial temperature remains relevant. In gas turbines, pre-cooled coolant [7] or steam cooling [8,12] is used, which is not very effective. The use of advanced thermal barrier coatings technologies [9,11] in gas turbines and monocrystalline superalloys [10,13,14] has not produced the desired temperature gradients and is unpredictable. The search for new cooling schemes [2] and the use of phantom cooling in gas turbines [15] are ineffective.

One way to remove heat from heat-stressed surfaces in a reliable way is to use various kinds of intensifiers [16], as well as porous [17,18] and microchannel cooling [19–21]. However, in [16–21], no data are given about how the cooling system of stationary gas-turbine units would be able to operate at initial gas temperatures of 1500 °C and more, or about the possibility of boosting [22]. Even the porous ceramic coating for transpiration cooling of gas turbine blades has proved ineffective [16]. Hybrid micro-nanomodulated

porous cooling surface is very expensive [17] and is unable to cope with high thermal loads. The results of the numerical simulation [18] have not been verified by testing. Among the heat transfer intensifiers used were rib-and-skin cooling in the gas turbine blade [19,20] and ribbing [21], but the heat transfer distribution was asymmetrical.

The main idea of the research is to transition from the boiling crisis to the limit state of heat exchange (walls and coatings). In earlier works [5,22], due to various heat exchange intensifiers, the authors expanded the limits of heat flow diversion several times and created a new cooling system. However, at the onset of the boiling crisis, the various authors, for example, in the sources we cited [23–46], did not study the limiting condition of the heating (cooling) surface. Researchers were interested in boiling crises of different kinds (first, second, third) of both a hydrodynamic and a thermodynamic nature. The strength characteristics of various capillary-porous coatings were determined by different authors in static and low-temperature modes (at room temperature).

Studies on homogeneous and inhomogeneous porous coatings [23], including hysteresis phenomena [24] and wick thickness effects [25], are still relevant, but the increase in critical flow is insufficient, although thermal contact resistance has been minimized compared to large volume boiling [26,27] and in honeycomb porous media [28]. The mechanism of boiling processes [26,27,29], including individual characteristics [26], the concept of phase separation [27], sub-cooling [30,31] and orientation [32], are of interest, but are difficult to apply to our studies.

Research on heat pipes as microchannel loop devices [33–36] aims to increase the capillary potential, which prevents heat flows involving different combined fields from dissipation. It includes mass forces (fields), especially for grooved wicks [34,41–43], sintered media [35,45], wick-ribbed and wick-grooved interfaces [36], powder coatings [37–39], and nanoparticle coatings [44]. Studies have also been carried out on pure and multi-component mixtures [40].

In this regard, the object of the research was a new system that allows control of the heat exchange by the combined action of capillary and mass forces and its thermohydraulic characteristics. The main purpose of this system is to increase the boost of heat transfer and to expand the limit of heat removal, that is, the critical values in porous coatings.

These studies are important for doctoral students, teachers, researchers, and manufacturers, as they help to solve problems in various thermal power plants of the intensification of heat transfer and the removal of high thermal loads. This brings production closer to being environmentally friendly, and the cooling system itself has undeniable advantages over conventional systems.

2. Field of Application of the New Capillary-Porous System

Figure 1 presents the methodology for porous systems design as applied to the developed devices of thermal power plants. The conducted research [5,22] makes it possible to introduce the coolant, body and structure material and type of porous coating, to carry out calculations of heat distribution, resistance, thermal stresses and to give an economic and ecological assessment.

To control the energy processes, it is proposed to divide the total energy into two components: the heat wave energy of the explosively generated steam nucleus and the energy of the compressed steam flow, which is also important for modeling and as an analogy of the boiling processes in the pores of the structure (the coating).

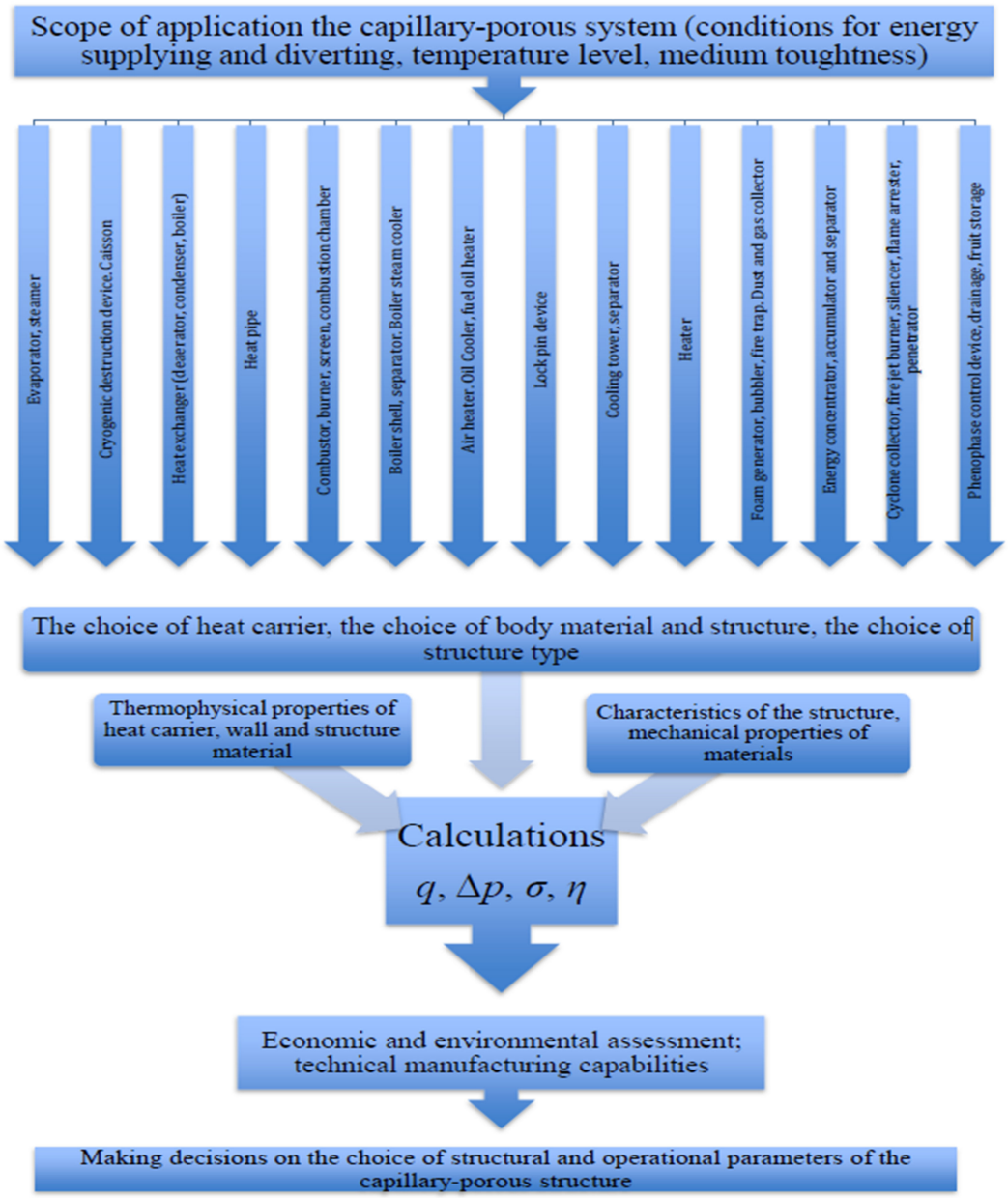

Figure 1. Block diagram of capillary-porous system design.

3. The Method. The Experimental Unit

The system shown in Figure 2 can operate in a closed cycle of the evaporation–condensation circuit or be open. The operating principle of the installation was as follows: the electric energy was supplied to the main heater from a welding transformer (WT), the output voltage of which equaled the following fixed values: 2.5; 5; 7.5 and 10 V. The electric current feeding the heater was measured using a universal transformer (UET) circuit.

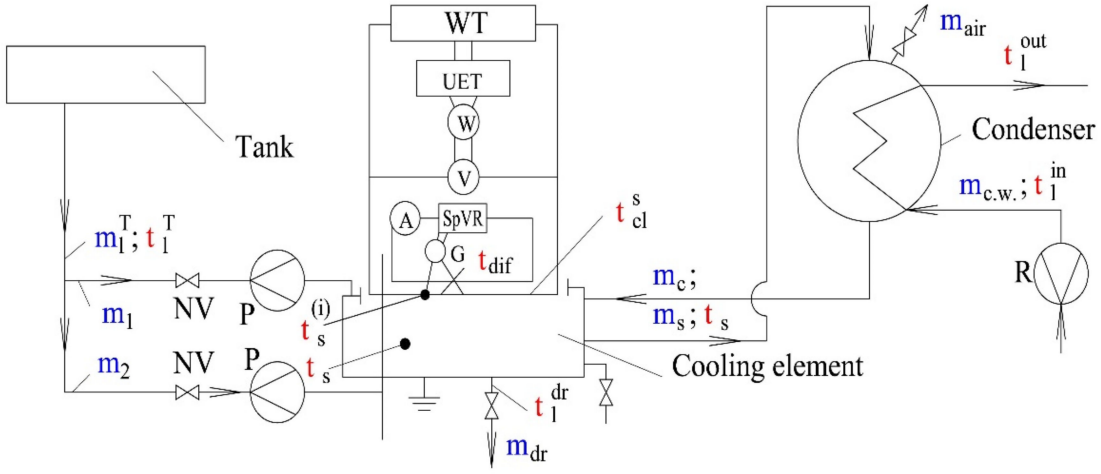

Figure 2. Experimental determination of heat fluxes on a heat exchange surface and capillary-porous structures (coating).

Secondary current was about 5 A, primary current was 100–2000 A. The voltage drop across the heater was measured with a voltmeter. The maximum possible inaccuracy in measuring current was ±0.6%, voltage drop ±1%, power ±1.6%. Electric energy was supplied to the security heater from the voltage regulator (SpVR).

The flow rates of the cooling and circulating liquids were determined by electric rotameters with a secondary electronic device calibrated by the volumetric method. The flow rates of the draining liquid and condensate were recorded using a measuring tank with a scale of 0.5×10^{-3} l, and the filling time was recorded using a stopwatch with a measuring sensitivity of 0.1 s. The possible inaccuracy in determining the liquid flow rate by rotameters did not exceed ±3%, and by the volumetric method did not exceed ±2%.

The studied surface was heated by a nichrome heater and cooled by a special cooling element. In the case of studying heat transfer through a metal wall without structures (coating), it was separated from a nichrome heater by mica. The structures were composed of one, two, and three layers of metal grids, and the coatings were sprayed using the plasma method (Figure 3).

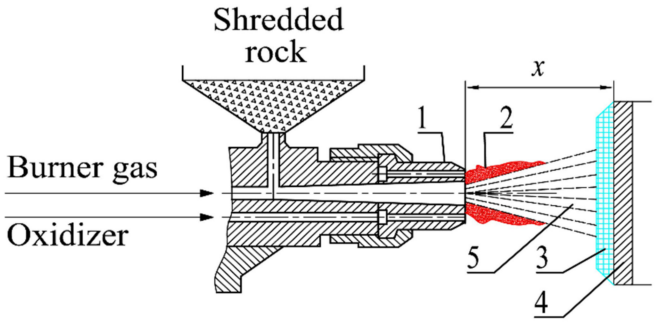

Figure 3. Spraying of a capillary-porous coating: 1—nozzle; 2—gas flame; 3—capillary-porous coating; 4—sprayed surface; 5—dispersed particles (quartz, granite, tesenit); *x*—is the distance determined by experience, depending on the mineral medium material.

The coatings were sprayed on the heat exchange surface (metal wall) with a gas flame rocket burner at a temperature of 2500–3000 °C and a flow velocity of 2000 m/s, using a fine fraction (peel). Coating modes were carried out with the following burner parameters, as described in Figure 3: oxygen consumption—18 nm^3/h; kerosene consumption—12 L/h.

4. The Model of the Boiling Crisis in Mesh Structures

The model of the boiling crisis is presented in the form of equations of continuity and motion, taking into account the combined action of gravity and capillary forces, while the gravity forces create an excess of liquid $\widetilde{m} = \frac{m_s}{m_l}$:

$$\frac{dV_y}{dy} = \frac{\rho_s L}{\rho_l \varepsilon F_w} V_x \left(\frac{m_s}{m_l} + 1 \right), \tag{1}$$

$$V_y \frac{dV_y}{dy} = g cos\beta + \frac{2\sigma d}{\rho_l dy} \left(\frac{1}{R_{(y)}} \right) - \frac{\varepsilon v_l V_y}{K}. \tag{2}$$

Substituting Equation (1) in Equation (2), taking into account the values: $V_y = \frac{G_{l(y)}}{\rho_l}$, $V_x = \frac{q_{cr}}{r\rho_s}$, and integrating the resulting equation in the range from $y_1 = 0$ to $y_2 = H$ and from $R_0 = \infty$ to $R_h = \frac{b_h}{2}$, we get:

$$\frac{3{q_{cr}}^2 h^2 \left(\frac{m_s}{m_l} + 1 \right)}{2(r\varepsilon\delta_w\rho_l)^2 \varphi'_{cr}} - \frac{3q_{cr} h^2 v_l}{2r\varepsilon\delta_w\rho_l K\varphi'_{cr}} + \left(g cos\beta + \frac{2\sigma}{\rho_l R_h} \right) = 0. \tag{3}$$

The solution to quadratic Equation (3) is an expression that determines the critical density of the heat flux of a slightly warmed and saturated liquid ($\widetilde{m} \to 1$):

$$q_{cr} = \frac{[B \pm (B^2 - 4AC)^{0.5}]}{2A}, \tag{4}$$

$$A = \frac{3h^2 \left(\frac{m_s}{m_l} + 1 \right)}{2(r\varepsilon\delta_w\rho_l)^2 \varphi'_{cr}}, \tag{5}$$

$$B = \frac{3h^2 v_l}{2r\varepsilon\delta_w\rho_l K\varphi'_{cr}}, \tag{6}$$

$$C = gHcos\beta + \frac{2\sigma}{\rho_l R_h}. \tag{7}$$

The experiment and calculation for q_{cr} values (Equation (4)) and the corresponding ΔT_{cr} values for various pressures are summarized in Table 1. For physical reasons, we leave the « − » sign in Equation (4). The initial calculation data were as follows: H = 10 m, $\cos\beta$ = 1; $R_h = 0.275 \times 10^{-3}$ m; h = 0.27 m; φ'_{cr} = 0.1; $\delta_w = 1.5 \times 10^{-3}$ m; $K = 5.8 \times 10^{-10}$ m^2.

Table 1. Critical heat loads (q_{cr}) and temperature head (ΔT_{cr}).

	***P*, MPa**			
	0.01	0.1	8	20
q_{cr}, W/m^2				
$K = K_{h.p.}$	2.95×10^4	6×10^5	6.9×10^5	1.66×10^5
$K = K_c$	3×10^5	6×10^5	2.5×10^5	5.8×10^3
ΔT_{cr}, K	14.2	60	55.2	7.75

The value of ΔT_{cr} in the porous structure characterizes the stability of the system. Assessment of ΔT_{cr} is connected with the difficulty in determining the effective coefficient of thermal conductivity at the time of boiling crisis, depending on the presence of a steam-water mixture in the boundary layer, contact resistance between the structure skeleton and the wall, and between the elements of the skeleton itself.

The thickness of the liquid layer is an uncertain value and the calculation of ΔT_{cr} cannot be performed analytically and has been the subject of experimental studies (see Table 1).

In the case of excess fluid, the $\widetilde{m}$ part of it can freely drain on the outer surface of the porous body, then it is necessary to introduce the conditional permeability coefficient K_c.

For high pressures, a stronger influence of the P value on the q_{cr} value is observed since the rapid drop in the coefficient σ begins to affect it. The presence of a gravitational potential can expand the q_{cr} value and stabilize the dependence $q_{cr} = f\ [P]$ for a wide range of pressure changes (0.01 . . . 20 MPa).

The moisture content φ affects q_{cr} through the ratio $\widetilde{m}$, and φ'_{cr} = (0.1 . . . 0.15). The experiments (see Table 1) were consistent with Equation (4), which was obtained based on the hydrodynamic analysis of heat transfer processes, where local restrictions on the heat flow were not taken into account when contact of the liquid film with the surface was excluded due to the intensive overheating of this surface during steam bubble growth. The disagreement with the theory is ±10%. The consideration that the hydrodynamic possibilities of heat transfer occur only in the presence of a fluid flow rate that exceeds (1.5 . . . 2) times what is needed, depending on the type of structure, is legitimate.

In this case, the specific heat fluxes were diverted in the system (2 . . . 8) times larger than in the heat pipes when using a mesh structure with intensive bubble boiling. In the capillary supply, the specific mass fluid flow of fluid G_{cr} was restricted to the limiting value of the capillary pressure and determined the hydrodynamic boundary of the heat transfer capacity. There was no such restriction for the combined action of forces, and G_{cr} was determined by the value of the effective pressure:

$$\Delta P_{cap+g} = \rho_l g H + \frac{2\sigma}{R_{min}}\ . \tag{8}$$

For engineering calculations, when the specific heat flux is diverted to q_{cr} with an intensive boiling process, Equation (4) can be used. To do this, it is necessary to know the pressure value, the geometry of the cooling system and the type of porous structure.

5. Unified Burner

In order to further unify the burners for the use of different fuel components (oxygen + kerosene; air + kerosene; air + gasoline), simplify the design, improve the reliability of cooling, ensure stable combustion of fuel of different compositions under any temperature conditions and increase the temperature of combustion products, the nozzle device and the burner shell were designed as a capillary-porous structure. The energy splitter of the gaseous oxidizer was designed as a high-pressure vortex chamber using the Ranque–Hilsch effect while the chamber was provided with a nozzle, and there were holes for the oxidizer withdrawal. In order to obtain the main mass of the oxidizer sharply cooled, the nozzle of the energy separator was made cylindrical, annular and supersonic. More efficient heating of fuel was provided by the fact that in the bottom part of the energy separator chamber outlet holes are made.

The burner (Figure 4) consisted of a combustion chamber 1 with a nozzle 2, which were made of capillary-porous material on the outside 3 (heat-resistant fabric, porous ceramics, capillary grooves on the walls of the combustion chamber and nozzle, mesh materials, mineral coatings, metal fiber, powder structures, etc.), and the outer casing 4, welded to the combustion chamber. The outlet holes were made in the bottom part of the combustion chamber. The capillary porous structure 3 was impregnated with liquid (water, methyl, glycerin, fusible metal, and others). A gap was left between the casing and the porous metal 3, from which air was pumped out after assembly.

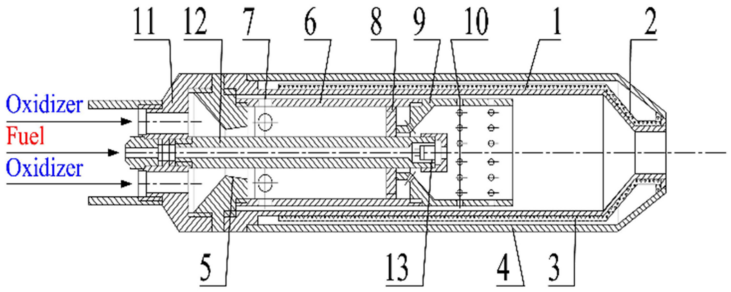

Figure 4. Unified burner, equipped with capillary-porous cooling structure (coating) and high-pressure vortex chamber with supersonic annular nozzle: 1—combustion chamber; 2—nozzle device; 3—capillary-porous coating; 4—casing; 5—nozzle; 6—vortex chamber; 7—outlet openings for cold flow removal; 8—outlet openings for hot flow removal; 9—fore-chamber; 10—oxidant supply openings; 11—main channel; 12—fuel supply pipe; 13—nozzle.

Combustion chamber 1 with nozzle 2 and casing 4 were screwed on the nozzle 5, on which the vortex chamber 6 was mounted. Nozzle 5 with a vortex chamber 6, in which the holes 7 and 8 were made to divert the cold and hot streams, formed a high-pressure energy separator of gaseous oxidant. The back of chamber 6 was adjacent to the prechamber 9 with holes 10 for the supply of oxidizer. For fuel supply, a tube 12 with nozzle 13 were screwed into the head. The gaseous oxidant entered the vortex energy separator through the head channels 11 and the nozzle 5 and divided itself into hot and cold components.

The hot stream flowed through the openings 8 and 10 into the pre-chamber, pre-washing the pipe 12, the nozzle 13 and heating the fuel. The larger part of the cooled oxidizer left the energy separator through the openings 7 and entered the combustion chamber 1. Part of this oxidizer passed through holes 10 into the prechamber 9, where it mixed with the atomized fuel and formed a fuel mixture. The combustion products were ejected through the nozzle 2. When the burner was in operation, the nozzle 2 and the area of the combustion chamber 1 adjacent to it were the most heat stressed.

When the walls of nozzle 2 and the combustion chamber 1 were heated, the coolant impregnating the porous material 3 took away heat from the walls, evaporated and rushed to the rear of the burner, washed from outside by a cold stream of oxidizer coming through the holes 7 of the energy separator. In the rear part of the capillary-porous system 3 there was condensation of the coolant, which returned to the hot walls of nozzle 2 and combustion chamber 1 through the capillaries. Afterwards the process was repeated.

6. Comparative Evaluation of System Investigated

Here is a comparative evaluation (Figure 5) of the investigated capillary-porous cooling system (4) with a curve in a large volume (area 1), thin-film evaporators (area 3) and heat pipe operation area (2). The system (4) extends the limit of heat load removal, approaching the boiling of liquid in a large volume, and in the case of application of intensifiers, it can withdraw large heat flows (shaded part of area 4).

The following elements were investigated as heat exchange intensifiers: corrugated porous elements with gaseous-liquid dispersoids and optimized capillary-porous structure; vibrating highly heat conducting branches and flexible turbulizers. Estimation of temperature difference $\Delta T = T_w - T_s$ in the porous structure is necessary for stable operation of the cooling system.

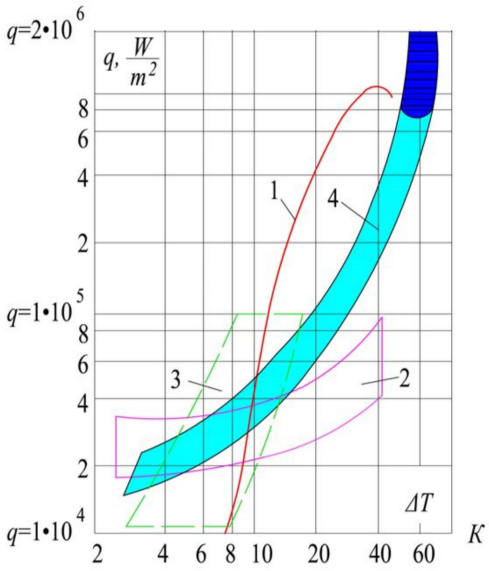

Figure 5. Dependence of the heat load on the overheating in relation to the water vapor temperature (1–4): 1—large-volume boiling on an uncoated surface [17,25,27–31,35,37,38,41,42,44]; 2—heat pipes operational area [18,23,24,26,32–34,36,39,43,45] with mesh wicks; 3—thin-film evaporators operational area [10]; 4—capillary-porous cooling system investigated. Shaded area—application of intensifiers in the porous system [15,40].

Such an assessment is quite complicated due to the difficulty of determining the effective thermal conductivity coefficient at the time of boiling crisis, which depends on many factors, the main ones being the presence of vapor–water mixture in the boundary layer, contact resistance between the structure skeleton and the wall and between the elements of the skeleton itself, which can vary, depending on the degree of the pressing of the structure to the wall and on the temperature level change of operation, which leads to thermal expansion of the wire mesh.

In addition, in the crisis mode, the thickness of the fluid layer is uncertain. Therefore, the calculation of q_{cr} value cannot be performed analytically and was the subject of experimental studies.

In addition, in the crisis mode, the thickness of the fluid layer is uncertain. Therefore, the calculation of q_{cr} value cannot be performed analytically and was the subject of experimental studies. To study the heat-transfer capabilities of capillary-porous systems, experiments were conducted for structures assembled from stainless steel metal meshes of 12X18H10T grade with different cell sizes (Table 2).

Table 2. Thermal transfer capabilities of q_{cr} investigated capillary-porous structures, heat pipes and thin-film evaporators.

Type of Capillary-Porous Structure	Heat Load q, 10^4 W/m^2					
	2	4	10	20	40	60
Temperature Pressure ΔT, K						
0.08 × 0.14 × 0.14	5.2	13.4	20.5	37.1	50	Wall burning
0.55	6.5	16.4	22.7	53.3	61	Wall burning
2 × 0.55	7.4	18.2	23.4	50.3	57	60
2 × 1	8.1	19.3	24.7	55.6	62.4	Wall burning
Heat Pipes						
0.08 × 0.14 × 0.14	2.5	10	40	Wall burning	Wall burning	Wall burning
2 × 0.55				Inoperable		
Thin-Film Evaporators (Without Capillary-Porous Structure)						
	3.7	5.7	8	Wall burning	Wall burning	Wall burning

7. Discussion of Experimental Data

Steam bubbles are deformed by the excess liquid $\widetilde{m}$ in the porous system, responsible for directing the movement to the flow V. In addition, their diameter is reduced and they are formed with greater frequency.

The energy that moves the boundary layer liquid near the wall is increased with the increase of flow velocity V. Therefore, the speed of steam generation V_{cr}, and the value of q_{cr} increase as well. However, the parameter $\widetilde{m}_{cr}$ determines such values of the liquid flow, which lead to a heat exchange crisis $q_{cr.v}$. due to insufficient energy to take out the liquid from the two-phased wall layer. The higher the flow values, the stronger the heat exchange crisis $q_{cr.v}$ will be. When moisture consumption reaches the value $\overline{\varphi'}_{cr}$, not only will the flow fail to contribute to increasing the value of q_{cr}, but it can even lead to a decrease of q_{cr} in some cases, making it difficult to evacuate steam from the wall area [5]. When the parameter $\widetilde{m}$ accelerates the speed of the liquid film next to the wall, the influence of the decline in moisture content $\overline{\varphi'}$ in the same area will start to prevail. Subsequently, it will affect to a large extent the value of q_{cr}, even reducing it. That is why it is required to determine the best ratio of excess liquid $\widetilde{m}$, in terms of the porous structure. When the balance of the acting forces is disturbed, the quantity of the liquid flowing in diminishes and it causes the appearance of «dry» spots on the heating surface K_{min}. The slow increase of the wall temperature causes the process to take place at temperature pressure (60 . . . 80) K, and growing F_s/F. The pulsating mode of supplying liquid to the surface prevents it from burning despite the diminishing intensity of the heat transfer. However, the pulsations in the wall temperature cause destructive thermal pressure, which shortens the service life of the surface. Hence, the optimization of the porous structure is important, as is preventing strong overheating of the wall, compared to the liquid temperature [22].

The selected minimum size of the mesh was 0.08×10^{-3} m, since smaller meshes would not allow the organization of bubble boiling and would be clogged by steam bubbles. The largest cell size was chosen to be 1×10^{-3} m, because the near zero capillary potential of larger cells results in non-uniform liquid distribution in the pores of the structure. The boiling crisis is determined by overburning of the wall. Optical methods based on holographic interferometry and high-speed filming with the SKS-1M camera were used to study the crisis phenomenon [5].

Mesh structures were formed from several layers of meshes. With a capillary-porous structure of 2×0.55, the greatest heat flows are dissipated by the combined action of mass and capillary forces. A structure consisting of a single 0.55×10^{-3} m mesh layer reduces the stability of the liquid film on the surface. When the number of mesh layers exceeds two, the wall is significantly overheated in terms of the steam temperature, and the crisis phenomena occur at an earlier stage. Moreover, no significant purification is required for the increased cell size (e.g., heat pipes) and water can be used [22]. The dissipated heat flow of the proposed structure is six times greater than that achieved in heat pipes and thin-film evaporators. Wall burn occurs as a result of steam bubbles clogging mesh cells, thus preventing fresh flow of liquid to the heated pipe surface. Despite the sufficient liquid excess m, $q_{cr.v.}$ occur and the critical values of liquid G_{cr}, vapor V_{cr} and their corresponding flow rate φ_{cr} and the limiting value of the «dry» spot K_{min}. If the wall is not coated by a capillary-porous structure and cooling is performed by a steam–water mixture at heat flows of about 1×10^5 W/m, the liquid film formed on the wall breaks up into individual jets and drops, which leads to overburning of the wall. The heated surface is not cooled by liquid coming from the core of the moving steam-water flow, so a film of steam is permanently formed on the inner side of the surface. Sharp deterioration of the heat transfer intensity, as well as variable temperature distortions, occur on the wall and this significantly worsens the conditions of heating surfaces, leading to their destruction [5].

A generalization of the experimental data made it possible to obtain the calculated equation for q_{cr} in the case when $P \geq 0.1$ MPa, a $b_h > 0.28 \times 10^{-3}$ m:

$$q_{cr} = 0.0347r \cdot \left[g \cdot (\rho_l - \rho_s) \cdot \rho_s \cdot \overline{D}'_{o.cr.}\right]^{0.5} \cdot \left(\frac{b_h}{b_0}\right)^{0.3} \cdot \left(\frac{\delta_f}{\delta_0}\right)^{0.5} \cdot (1 + cos\beta)^{0.6}, \quad (9)$$

where $\overline{D}'_{o.cr.}$—average breakaway (destructive) diameter of the bubble (conglomerate) at the moment of heat transfer crisis.

$$\overline{D}'_{o.cr.} = \left[\frac{\rho_l}{g \cdot (\rho_l - \rho_s)}\right]^{\frac{1}{3}} \cdot \left[8.94 \times 10^{-2} \cdot \left[\frac{\tau^2 \cdot T_s}{r \cdot \rho_l \cdot \rho_s}\right]^{\frac{1}{3}} + 15.3 \cdot \left[\frac{\lambda_l}{r \cdot \rho_s}\right]^{\frac{2}{3}}\right], \quad (10)$$

$\overline{D}'_{o.cr.}$—obtained by processing cine-photographs. The divergence (correlation) of theory and experiment is ± 10 %. The investigated capillary-porous mesh structure of 2 × 0.55 type takes away heat flows of significant proportions. This becomes possible because the capillary and mass forces ΔP_{cap+g} in the structure volume act in unison, which facilitates the destruction of vapor conglomerates in the pores. Visualization of the process [5] showed that cold liquid portions exist in the cell structure and they rush to the border zones, destroying steam bubbles. Turbulization of two-phase boiling stable pulsating boundary layer is taking place. The guiding partitions inside the tubes add to an inflow of fluid to the structure surface, because of the impact they have on the centrifugal forces flow when they bend the transverse porous partitions.

The influence of the mesh width on q_{cr} value is shown in Figure 6. The calculation is made according to Equations (4) and (9). Mesh and wall are made of stainless steel. The experiments were carried out for the following conditions: h = 0.27 m; $\widetilde{m}$ = optimal; P = 0.1 MPa; β = 0 deg. Excess fluid is calculated according to the formulas:

$$\text{for } b_h \leq 0.28 \times 10^{-3} \text{ m}, \frac{m_l}{m_s} = 1.3 \div 2;$$

$$\text{for } b_h > 0.28 \times 10^{-3} \text{ m}, \frac{m_l}{m_s} = 1.5 \div 2.5.$$

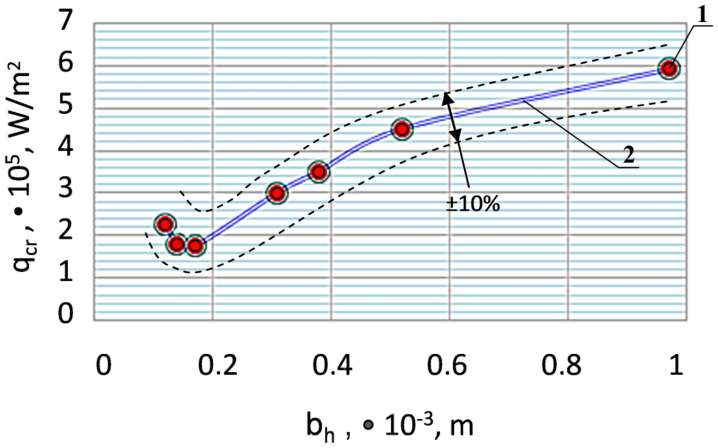

Figure 6. The dependence of the critical heat flow rate per unit area (q_{cr}) on the mesh width (b_h) during water boiling: 1—experiment; 2—calculations according to Equations (4) and (9).

For water boiling in a large volume at atmospheric pressure, the critical wavelength λ_{cr} between the steam columns is (15–25) × 10^{-3} m, then for a powder porous coating it is 5–15 times smaller. If the value of $q_{cr} \sim U_{cr} \sim \lambda_{cr} - 0.5$, then the value of q_{cr} for powder materials turned out to be twice as high, but at a temperature head ΔT = 600–800 K. For grid structures operating in the field of gravitational forces, in spite of an even smaller

value of λ_{cr}, the value of q_{cr} was similar to the values achieved at boiling in a large volume on the technical surface, but at a value of ΔT_{cr} = 60 K [22], U_{cr}—critical velocity of steam. Therefore, the hydrodynamic situation in the volume and on the surface of the grids, which, in turn, depends on the type of structure, and organization of the liquid supply should be considered as the determining factor of the boiling crisis. Due to a slight surplus of liquid, as visual observations showed, it became possible to control the steam front in the volume of the structure and, above all, to destroy the accumulating steam formations. An assessment for crisis state of the fraction of the surface occupied by the steam for P = 0.1 MPa, ΔT_{cr} = 60 K, $\overline{D}'_{o.cr.}$ = 0.5 × 10^{-3}, $\widetilde{m}$ = 1.1, $\overline{n}$ = 5 × 10^6 m^2, is provided by the following:

$$\frac{F_s}{F} \geq \frac{\pi \overline{D}'_{o.cr.}\, \overline{n} K_{min}}{4.1} \geq \frac{2.5\pi}{16}, \quad (11)$$

where K_{min} is the coefficient, taking into account the presence of a dry spot under the steam bubble. At the time of the crisis, the value of $K_{min} \geq 0.5$, F, F_s—the total heat exchange surface occupied by steam [22].

The number of cells for the structure of 0.4 × 10^{-3} m, per 1 m^2, is 2.78 × 10^6 pcs, that is, at the time of the crisis there may be two steam bubbles in each cell. When the liquid is boiling in a large volume for a horizontal heater with a technical surface in the theory of hydrodynamic crisis, the ratio is Fs / F = π/16, i.e., 2.5 times less. When the value of $K_{min} \rightarrow 1$, the ratio $Fs/F \rightarrow 1$. Geometric dimensions that significantly affect redistribution of the capillary and gravitational potentials affect the value $q$cr and thus require optimization. The maximum value of $q$cr was obtained for vertical surfaces with large cell sizes ($\beta = 0^\circ$), where β is the angle of inclination of the surface to the vertical line, Equation (4). Thus, the essential dependence of the heat transfer ability of the studied system from the width of grid (dozens of times), as it takes place in the heat pipes, was not observed. This can be explained by the fact that at small sizes of cells in the presence of gravitational forces, high hydraulic resistance limits consumption to a lesser extent, which can partially flow over for grid surface. At the same time, increased cell size does not lead to a significant decrease of transfer capacity. However, the width of a grid cell in the system under study affects the dynamics of the steam bubbles' development and hence the intensity of the heat exchange and the value of the $q$cr. The behavior of bubble formation in individual cells (isolated), as was the case in the system under study, prevents premature fusion of steam bubbles and the formation of a solid steam film. The presence of large cells allows us to improve the ejection of the light phase from the steam-generating surface. However, it is not advisable to increase the cells' size starting from a width of 0.4 × 10^{-3} m, as steam conglomerates occur in such cells, similar to boiling on a technical surface without a porous coating [22].

8. Conclusions

The studied capillary-porous system yields much better results than the traditional pool boiling because the two forces—capillary and mass—act simultaneously. In the new proposed system, the intensity of exchanging heat and mass can be controlled and accelerated to a greater extent. This synergy of the material is a real improvement to the existing cooling systems. The developed nano- and micro-scale structured surfaces in the form of coatings and mesh structures have the integrated effect of industrial meshes with natural (natural) mineral coatings and have the synergistic advantages of combining these two developments in an integrated technology of their pro-duction, expansion of critical thermal loads and management of the border state of porous coatings.

Although both capillary-porous and flow-through burner cooling systems have performed equally efficiently in terms of cooling the metallic parts of combustion chambers and nozzles (1 × 10^6 W/m^2), the former is much more environmentally-friendly. For each heat flow, the thickness of the coating, which plays a role in the process of energy transfer, has been determined. Similarly, the energy with which the individual coatings are

destroyed by the respective heat flow has also been estimated. A granite coating would be destroyed by the energy of a limiting value of up to 2.5×10^9 J/m^3.

A possible practical implementation of the results we have obtained would be preventing the destruction of gas turbine surfaces heavily affected by heat flows. Our research on selecting the best polycrystal natural environment and modelling it accordingly is extremely valuable for practice. The results obtained can be extended to the modernization of chimneys, cooling towers made of reinforced concrete, and the work is conducted with the environment in mind (the cooling agent consumption being reduced dozens of times). The prospects for research of burners with energy separator in the form of a vortex chamber with capillary-porous coatings have been determined.

It is shown that the model of hydrodynamic crisis developed by the authors (Equations (1)–(4)) for the new capillary-porous cooling system, operating in the field of capillary and mass forces, reflects well the influence of pressure P in the system for the onset of critical loads q_{cr} and wall overheating ΔT_{cr}, while the pressure varies within a wide range $(10^{-2} \div 2 \times 10^1)$ MPa. It is shown that a good match between theory and experiment is accounted for by the thermophysical properties of the coolant, directly derived from the model (Equations (1)–(4)), rather than from an empirical account of the pressure parameter P.

A comparative evaluation of the newly studied structures confirms their advantage over other cooling systems (see Figure 5). The lower intensity of heat exchange of the studied system compared to boiling in a large volume can be explained by the theory of micro-layer evaporation, when the main share of heat is brought to the base of the steam bubbles and is spent on evaporation into the bubbles. In the studied system this value is proportional to the temperature head $\Delta T = T_w - T_s \sim \Delta T^2$.

A comparison with heat pipes for $q > 100$ kW/m^2 shows that the intensity in the heat pipes is 40% lower, or they are not functional. With $q < 20$ kW/m^2 heat pipes have a high intensity. In the field of $(2 \ldots 10) \times 10^4$ W/m^2 satisfactory agreement with experimental data is observed.

Author Contributions: A.G.: Conceptualization, Experimental method, Methodology, Writing—original draft. H.B.: Supervision, Investigation, review & editing. D.B.: Experimental data, Mathematical model, Data creation, Investigation, Calculations. All authors have read and agreed to the published version of the manuscript.

Funding: This research received no external funding.

Institutional Review Board Statement: Not applicable.

Informed Consent Statement: Not applicable.

Data Availability Statement: Not applicable.

Conflicts of Interest: The authors declare no conflict of interest.

References

1. Miao, H.; Wang, Z.; Niu, Y. Key issues and cooling performance comparison of different closed Brayton cycle based cooling systems for scramjet. *Appl. Therm. Eng.* **2020**, *179*, 115751. [CrossRef]
2. Baakeem, S.S.; Orfi, J.; Al-Ansar, H. Performance improvement of gas turbine power plants by utilizing turbine inlet air-cooling (TIAC) technologies in Riyadh, Saudi Arabia. *Appl. Therm. Eng.* **2018**, *138*, 417–432. [CrossRef]
3. Wróblewski, W. Numerical evaluation of the blade cooling for the supercritical steam turbine. *Appl. Therm. Eng.* **2013**, *51*, 953–962. [CrossRef]
4. Singh, O.; Prasad, B.N. Influence of different means of turbine blade cooling on the thermodynamic performance of combined cycle. *Appl. Therm. Eng.* **2008**, *28*, 2315–2326. [CrossRef]
5. Genbach, A.A.; Bondartsev, D.Y.; Iliev, I.K.; Georgiev, A.G. Scientific method of creation of ecologically clean capillary-porous systems of cooling of power equipment elements of power plants on the example of gas turbines. *Energy* **2020**, *199*, 117458. [CrossRef]
6. Gou, J.J.; Chang, Y.; Yan, Z.W.; Chen, B.; Gong, C.L. The design of thermal management system for hypersonic launch vehicles based on active cooling networks. *Appl. Therm. Eng.* **2019**, *159*, 113938. [CrossRef]

7. Moon, S.W.; Kwon, H.M.; Kim, T.S.; Kang, D.W.; Sohn, J.L. A novel coolant cooling method for enhancing the performance of the gas turbine combined cycle. *Energy* **2018**, *160*, 625–634. [CrossRef]
8. Wang, W.; Gao, J.; Shi, X.; Xu, L. Cooling performance analysis of steam cooled gas turbine nozzle guide vane. *Int. J. Heat Mass Transf.* **2013**, *62*, 668–679. [CrossRef]
9. Schulz, U.; Leyens, C.; Fritxher, K.; Peters, M.; Saruhan-Brings, B.; Lavigne, O.; Dorvaux, J.-M.; Poulain, M.; Mévrel, R.; Caliez, M. Some recent trends in research and technology of advanced thermal barrier coatings. *Aerosp. Sci. Technol.* **2003**, *7*, 73–80. [CrossRef]
10. Zhang, J.X.; Harada, H.; Ro, Y.; Koizumi, Y.; Kobayashi, T. Thermomechanical fatigue mechanism in a modern single crystal nickel base superalloy TMS-82. *Acta Mater.* **2008**, *56*, 2975–2987. [CrossRef]
11. Clarke, D.R.; Phillpot, S.R. Thermal barrier coating materials. *Mater. Today* **2005**, *8*, 22–29. [CrossRef]
12. Wang, W. Efficiency study of a gas turbine guide vane with a newly designed combined cooling structure. *Int. J. Heat Mass Transf.* **2015**, *80*, 217–226. [CrossRef]
13. Zhong, Z.; Gu, Y.; Yuan, Y.; Yokawa, T.; Harada, H. Mechanical properties and fracture modes of an advanced Ni–Co-base disk superalloy at elevated temperatures. *Mater. Charact.* **2012**, *67*, 101–111. [CrossRef]
14. Zhang, J.X.; Murakumo, T.; Harada, H.; Koizumi, Y. Dependence of creep strength on the interfacial dislocations in a fourth generation SC superalloy TMS-138. *Scr. Mater.* **2003**, *48*, 287–293. [CrossRef]
15. Yang, X.; Liu, Z.; Liu, Z.; Feng, Z.; Simon, T. Turbine platform phantom cooling from airfoil film coolant, with purge flow. *Int. J. Heat Mass Transf.* **2019**, *140*, 25–40. [CrossRef]
16. Arai, M.; Suidzu, T. Porous Ceramic Coating for Transpiration Cooling of Gas Turbine Blade. *J. Therm. Spray Tech.* **2013**, *22*, 690–698. [CrossRef]
17. Khan, S.A.; Sezer, N.; Koç, M. Design, fabrication and nucleate pool-boiling heat transfer performance of hybrid micro-nano scale 2-D modulated porous surfaces. *Appl. Therm. Eng.* **2019**, *153*, 168–180. [CrossRef]
18. Yan, G.; Li, Z.; Bore, T.; Torres, S.A.G.; Scheuermann, A.; Li, L. Discovery of Dynamic Two-Phase Flow in Porous Media Using Two-Dimensional Multiphase Lattice Boltzmann Simulation. *Energies* **2021**, *14*, 4044. [CrossRef]
19. Kuzma-Kichta, Y.A.; Leontiev, A.I. Preface: Heat and mass transfer enhancement on macro-, micro-, and nanoscales. *J. Enhanc. Heat Transf.* **2018**, *25*, 2018. [CrossRef]
20. Choi, E.Y.; Choi, Y.D.; Lee, W.S.; Chung, J.T.; Kwak, J.S. Heat transfer augmentation using a rib–dimple compound cooling technique. *Appl. Therm. Eng.* **2013**, *51*, 435–441. [CrossRef]
21. Armellini, A.; Casarsa, L.; Mucignat, C. Experimental assessment of the aero-thermal performance of rib roughened trailing edge cooling channels for gas turbine blades. *Appl. Therm. Eng.* **2013**, *58*, 455–464. [CrossRef]
22. Genbach, A.A.; Bondartsev, D.Y.; Iliev, I.K. Heat transfer crisis in the capillary-porous cooling system of elements of heat and power installations. *Therm. Sci.* **2019**, *23*, 849–860. [CrossRef]
23. Ji, X.; Xu, J.; Zhao, Z.; Yang, W. Pool boiling heat transfer on uniform and non-uniform porous coating surfaces. *Exp. Therm. Fluid Sci.* **2013**, *48*, 198–212. [CrossRef]
24. Poniewski, M.E. Peculiarities of boiling heat transfer on capillary-porous coverings. *Int. J. Therm. Sci.* **2004**, *43*, 431–442. [CrossRef]
25. Li, C.; Peterson, G.P.; Wang, Y. Evaporation/Boiling in Thin Capillary Wicks (I)—Wick Thickness Effects. *J. Heat Transf.* **2006**, *128*, 1312–1319. [CrossRef]
26. Chang, Y.H.; Ferng, Y.M. Experimental investigation on bubble dynamics and boiling heat transfer for saturated pool boiling and comparison data with previous works. *Appl. Therm. Eng.* **2019**, *154*, 284–293. [CrossRef]
27. Sarwar, M.S.; Jeong, Y.H.; Chang, S.H. Subcooled flow boiling CHF enhancement with porous surface coatings. *Int. J. Heat Mass Transf.* **2007**, *50*, 3649–3657. [CrossRef]
28. Mori, S.; Okuyama, K. Enhancement of the critical heat flux in saturated pool boiling using honeycomb porous media. *Int. J. Multiph. Flow* **2009**, *35*, 946–951. [CrossRef]
29. Xie, J.; Xu, J.; Liang, C.; She, Q.; Li, M. A comprehensive understanding of enhanced condensation heat transfer using phase separation concept. *Energy* **2019**, *172*, 661–674. [CrossRef]
30. Krepper, E.; Končar, B.; Egorov, Y. CFD modelling of subcooled boiling-Concept, validation and application to fuel assembly design. *Nucl. Eng. Des.* **2007**, *237*, 716–731. [CrossRef]
31. Ose, Y.; Kunugi, T. Numerical Study on Subcooled Pool Boiling. In Proceedings of the ASME/JSME 2011 8th Thermal Engineering Joint Conference, Honolulu, HI, USA, 13–17 March 2011; ASME: Honolulu, HI, USA, 2011. [CrossRef]
32. Chuang, T.J.; Chang, Y.H.; Ferng, Y.M. Investigating effects of heating orientations on nucleate boiling heat transfer, bubble dynamics, and wall heat flux partition boiling model for pool boiling. *Appl. Therm. Eng.* **2019**, *163*, 114358. [CrossRef]
33. Yu, M.; Diallo, T.M.; Zhao, X.; Zhou, J.; Du, Z.; Ji, J.; Cheng, Y. Analytical study of impact of the wick's fractal parameters on the heat transfer capacity of a novel micro-channel loop heat pipe. *Energy* **2018**, *158*, 746–759. [CrossRef]
34. Odagiri, K.; Nagano, H. Investigation on liquid-vapor interface behavior in capillary evaporator for high heat flux loop heat pipe. *Int. J. Therm. Sci.* **2019**, *140*, 530–538. [CrossRef]
35. Hanlon, M.A.; Ma, H.B. Evaporation Heat Transfer in Sintered Porous Media. *J. Heat Transf.* **2003**, *125*, 644–652. [CrossRef]
36. Li, J.; Hong, F.; Xie, R.; Cheng, P. Pore scale simulation of evaporation in a porous wick of a loop heat pipe flat evaporator using Lattice Boltzmann method. *Int. Commun. Heat Mass Transf.* **2019**, *102*, 22–33. [CrossRef]

37. Alam, M.S.; Prasad, L.; Gupta, S.C.; Agarwal, V.K. Enhanced boiling of saturated water on copper coated heating tubes. *Chem. Eng. Process. Process Intensif.* **2008**, *47*, 159–167. [CrossRef]
38. Arik, M.; Bar-Cohen, A.; You, S.M. Enhancement of pool boiling critical heat flux in dielectric liquids by microporous coatings. *Int. J. Heat Mass Transf.* **2007**, *50*, 997–1009. [CrossRef]
39. Alekseik, O.S.; Kravets, V.Y. Phisycal model of boiling process on porous surface in limited space. *East. Eur. J. Enterp. Technol.* **2013**, *4*, 26–31. [CrossRef]
40. Jamialahmadi, M.; Müller-Steinhagen, H.; Abdollahi, H.; Shariati, A. Experimental and theoretical studies on subcooled flow boiling of pure liquids and multicomponent mixtures. *Int. J. Heat Mass Transf.* **2008**, *51*, 2482–2493. [CrossRef]
41. Das, A.K.; Das, P.K.; Saha, P. Performance of different structured surfaces in nucleate pool boiling. *Appl. Therm. Eng.* **2009**, *29*, 3643–3653. [CrossRef]
42. Li, C.; Peterson, G.P. Evaporation/Boiling in Thin Capillary Wicks (II) -Effects of Volumetric Porosity and Mesh Size. *J. Heat Transfer.* **2006**, *128*, 1320–1328. [CrossRef]
43. Boubaker, R.; Platel, V. Dynamic model of capillary pumped loop with unsaturated porous wick for terrestrial application. *Energy* **2016**, *111*, 402–413. [CrossRef]
44. Forrest, E.; Wiliamson, E.; Buongiorno, J.; Hu, L.-W.; Rubner, M.; Cohen, R. Augmentation of nucleate boiling heat transfer and critical heat flux using nanoparticle thin-film coatings. *Int. J. Heat Mass Transf.* **2010**, *53*, 58–67. [CrossRef]
45. Chernysheva, M.A.; Pastukhov, V.G.; Maydanik, Y.F. Analysis of heat exchange in the compensation chamber of a loop heat pipe. *Energy* **2013**, *55*, 253–262. [CrossRef]
46. Celik, M.; Paulussen, G.; Van Erp, D.; De Jong, W.; Boersma, B.J. Transient Modelling of Rotating and Stationary Cylindrical Heat Pipes: An Engineering Model. *Energies* **2018**, *11*, 3458. [CrossRef]